An Experimental Investigation of the Ion Storage/Transfer Behavior in an Electrical Double-Layer Capacitor by Using Monodisperse Carbon Spheres with Microporous Structure

ARTICLE *in* THE JOURNAL OF PHYSICAL CHEMISTRY C · DECEMBER 2012

Impact Factor: 4.77 · DOI: 10.1021/jp308415s

5 AUTHORS, INCLUDING:

Shunsuke Tanaka
Kansai University
75 PUBLICATIONS **1,861** CITATIONS

SEE PROFILE

THE JOURNAL OF PHYSICAL CHEMISTRY C

Article

pubs.acs.org/JPCC

An Experimental Investigation of the Ion Storage/Transfer Behavior in an Electrical Double-Layer Capacitor by Using Monodisperse Carbon Spheres with Microporous Structure

Shunsuke Tanaka,*[,†,‡] Hatsumi Nakao,[†] Takenori Mukai,[†] Yugo Katayama,[†] and Yoshikazu Miyake[†,‡]

[†]Department of Chemical, Energy and Environmental Engineering, Faculty of Environmental and Urban Engineering, Kansai University, 3-3-35 Yamate-cho, Suita-shi, Osaka 564-8680, Japan

[‡]Organization for Research and Development of Innovative Science and Technology (ORDIST), Kansai University, 3-3-35 Yamate-cho, Suita-shi, Osaka 564-8680, Japan

Supporting Information

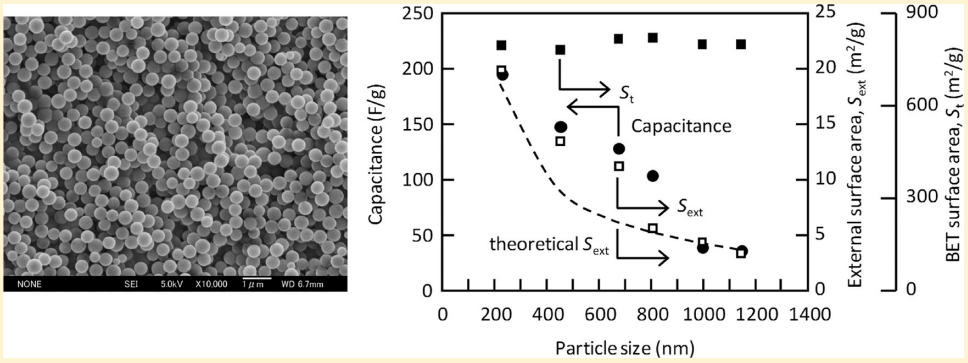

ABSTRACT: Monodisperse carbon spheres with coefficient of variation less than 4% were successfully synthesized through polycondensation of resorcinol with formaldehyde in the presence of ammonia as a catalyst followed by carbonization in an inert atmosphere. The diameters of the carbon spheres can be tuned in the range of 220−1140 nm by adjusting the ammonia concentration in the precursor solutions. Although the particle size decreases with increasing ammonia concentrations, there is no large difference in the internal pore structure between the different-sized carbon spheres. The size-controlled monodisperse carbon spheres were used as a model material to understand the ion storage/transfer behavior in electrical double-layer capacitor (EDLC). The present study clearly indicates that the reducing the particle size and highly monodispersity in both size and shape were effective at reducing mass transport resistance and improving EDLC performance reliability.

1. INTRODUCTION

Nanostructured carbon materials have attracted much attention because of their unique chemical, physical characteristics, and potential applications in strength-reinforcing additives, separation, adsorbents, gas storage, fuel cells, sensing, and catalyst supports.[1−19] The application functionalities of the carbon materials are concerned with the performance of the electrochemical and nanostructural properties. Electrochemical double layer capacitors (EDLC) are electrical storage media based on the physisorption of ions. The performance of EDLCs depends on the properties of the carbon materials, such as pore size, pore structure, surface functional groups, and electrical conductivity. Many researchers have focused on developing carbon materials with various unique structures, the most popular being carbon aerogels,[12,13] fullerenes,[1] nanotubes,[2] ordered microporous carbons,[4] ordered mesoporous carbons,[14−19] and inverse opal carbons.[6] Besides the variation of nanostructure, the morphological and size control of carbon materials has been a key breakthrough toward the development of practical applications. Various morphologies have been reported, including films, fibers, and spheres. However, it is difficult to draw a simple relationship between the structural and morphological properties of carbon materials and the EDLC performance because of the complicated structures and morphologies of the carbon materials.

It has been thought that great advantages for academic and industrial fields would emerge from size-controlled monodisperse spheres. The use of monodisperse spheres make it possible to give reliable and reproducible performances for their applications. Until now, many attempts have been made toward the synthesis of carbon microspheres, such as catalytic chemical vapor deposition, arc discharge, pressure carbonization, and catalytic pyrolysis of organic compounds.[20−24] Generally, these synthesis methods need complex equipment and rigorous conditions. In addition, the resulting products often have a broad distribution in size. In these vapor phase methods,

Received: August 24, 2012
Revised: November 27, 2012
Published: December 4, 2012

   dx.doi.org/10.1021/jp308415s | J. Phys. Chem. C 2012, 116, 26791−26799

synthesis of highly monodisperse carbon spheres remains challenging.

On the other hand, polymer and silica spheres are readily fabricated and commercially available with high monodispersibility. Development of techniques for producing polymer spheres has long been the subject of extensive work.[25−27] Various synthesis methods have been reported, including physical methods such as emulsification, coacervation, and spray-drying and chemical method such as heterogeneous polymerization. Most of particles for biologically relevant applications have been prepared by physical methods using natural polymers. However, particles obtained through physical methods often have a broad distribution in size. Typical method for producing monodisperse polymer spheres is heterogeneous polymerization, including precipitation, dispersion, suspension, and emulsion polymerization. The dispersion medium is generally water. A dispersion whose medium is not water is referred to as a nonaqueous dispersion. Most of heterogeneous polymerization systems are based on polyacrylamide-, polystyrene-, poly(methyl methacrylate)-, or polyaniline-related materials. The properties of spheres prepared by emulsion polymerization are decided by the monomers used, emulsifiers, and initiators. The emulsifier molecules play a role in improving the particle dispersion stability. However, the emulsifier molecules remain as a contaminant and cause particle coagulation during solid−liquid separation. To overcome these problems, two techniques—elimination of emulsifiers and use of polymerizable emulsifiers—have been proposed. On the other hand, Stöber method is well-known to produce silica spheres with low polydispersity.[28−30] In the system, silicon alkoxide is hydrolyzed and condensed in alcohol/water in the presence of a basic catalyst such as ammonia. Simple and novel liquid-phase methods inspired by the Stöber system, which use basic amino acids in place of ammonia, have recently been developed to synthesize uniform-sized silica nanospheres with particle diameters in the range 10−200 nm.[31] Interestingly, the ordered arrangement of silica nanospheres formed a well-ordered mesopore system.

The polymeric precursor offers many advantages such as widespread availability, easy modification, excellent shape forming, and high thermal stability. The choice of the polymeric precursor is the first important factor since pyrolysis of different precursors may bring about different kinds of carbon materials. Based on our experience with preparation of ordered mesoporous carbons,[16−19] resorcinol/formaldehyde resins are favorable carbon precursors, especially when a carbon with few inorganic impurities is needed. Resorcinol reacts with formaldehyde to form a cross-linked network. The major reactions between resorcinol and formaldehyde include (1) the addition reaction to form hydroxymethyl ($-CH_2OH$) derivatives of resorcinol and (2) the condensation of the hydroxymethyl derivatives to form methylene ($-CH_2-$) and methylene ether ($-CH_2OCH_2-$) bridged compounds through eliminating water molecules, resulting in cross-linked polymerized resorcinol/formaldehyde resin network. Interestingly, it has been pointed out that the polymerization mechanism and structure of resorcinol/formaldehyde under basic conditions are analogous to that described for the sol−gel processing of silica.[12] Although there has been considerable research on monodisperse polymer spheres, only a few articles dealt with the preparation of monodisperse spheres derived from resorcinol/formaldehyde resin.[32−34] To the best of our knowledge, Friedel et al. have prepared for the first time highly monodisperse submicrometer resin spheres by the condensation of melamine with formaldehyde in an aqueous solution followed by carbonization in an inert atmosphere.[32] For the polycondensation reaction between melamine and formaldehyde, formic acid was used as a catalyst. Scherdel et al. have reported the synthesis parameters of resorcinol/formaldehyde solutions with sodium carbonate toward the regime of nonmonolithic phases and individual separated particles.[34] Their results demonstrated that the formation of monodisperse spheres rather than monolithic gels is obtained for low sodium carbonate concentration and low mass content of resorcinol and formaldehyde in the starting solution. Dong et al. have reported a basic amino acid-assisted synthesis of resin nanospheres.[33] In their Stöber-like system, the resorcinol was condensed with formaldehyde in an aqueous solution in the presence of L-lysine or ammonia. The use of highly monodisperse resin spheres is thus very effective toward converting the monodisperse carbon spheres. Simple techniques to prepare highly monodisperse porous carbon spheres are required for the development of practical applications. Recently, an extension of the Stöber method for the preparation of monodisperse resorcinol/formaldehyde spheres with uniform and tunable particle size has been reported by Liu et al.[35] They mentioned that the pyrolysis of monodisperse resorcinol/formaldehyde resin spheres is suitable for preparation of monodisperse carbon spheres. In addition, their results demonstrated that the Stöber method approach is useful for the production of monodisperse carbon spheres. More recently, Liu's method was extended to the preparation of carbon−inorganic composite spheres in the presence of tetraethyl orthosilicate or silver nitrate by Choma et al.[36] However, the drawback of the synthetic route is that the hydrothermal procedure using a Teflon-lined autoclave is required after stirring the mixture at 30 °C because one cannot make any direct observation of the particle generation.

In this work, we examine the applicability of Stöber-like condition to producing the spherical resorcinol/formaldehyde resin particles. It is important to note that our synthetic route, reported here, does not require the hydrothermal procedure, which further resembles original Stöber method. On the other hand, it is totally different from the well-known Stöber method in that our synthetic route avoids an agitation operation in the formation of particles. We report the preparation and characterization of spherical phenolic resin particles by polycondensation of resorcinol with formaldehyde, and focus on the effects of solvent and ammonia catalyst on mean particle size, particle size distribution, and specific surface area. Another objective of this study is to reveal the mechanism of EDLCs by using the monodisperse carbon spheres as model materials. In theory, the capacitance of EDLCs should be proportional to the specific surface area of carbon materials. However, many studies have shown an unfavorable divergence from this linear relation. Among the resistance components, the ion transfer in the electrode pores governs the total resistance.[37,38] With increasing charge/discharge rates the capacitance contribution from the micropores diminishes rapidly due to mass transport resistance effects. The above reports suggest that control of the size of carbon spheres is a very important factor in improving the capacitance and the rate performance of EDLCs. The effect of particle size would become more apparent if size-controlled monodisperse carbon spheres with uniform specific surface area were used as model electrodes.

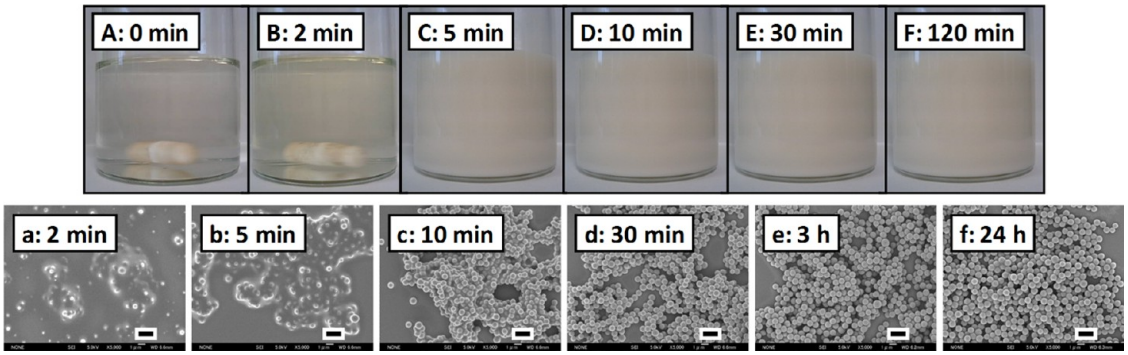

Figure 1. Photographs of the solutions (A–F) and FESEM images of the products (a–f: scale bar; 2 μm) with time after the addition of ammonia. The products were prepared at ethanol concentration of 40 vol % and ammonia concentration of 0.15 mol/L.

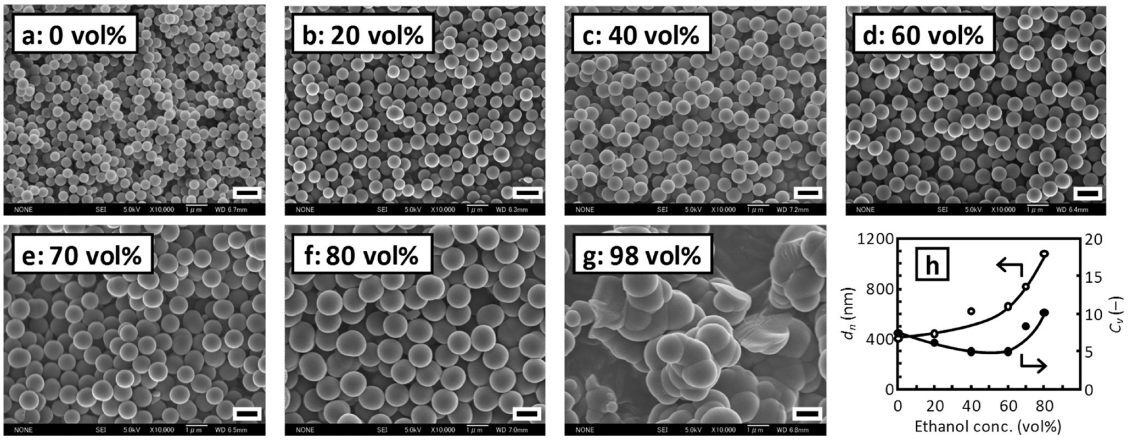

Figure 2. FESEM images of resorcinol/formaldehyde resin particles prepared at different ethanol concentrations (a–g: scale bar; 1 μm). Effect of ethanol concentration on the d_n and C_v of spherical particles (f). The products were prepared at ammonia concentration of 0.15 mol/L.

2. EXPERIMENTAL SECTION

2.1. Chemicals. Resorcinol, formaldehyde (36–38 wt %), ammonia solution (10 wt %), methanol, ethanol, and isopropanol were purchased from Wako Pure Chemical Industries and used as received. Pure water with conductivity of less than 1 μS/cm was obtained by using a RFD210PA pure distillation apparatus (Advantec Co. Ltd.).

2.2. Synthesis of Monodisperse Resorcinol/Formaldehyde Resin and Carbon Spheres. Phenolic resin particles were prepared by polycondensation reaction of resorcinol with formaldehyde in alcohol/water. Resorcinol was completely dissolved in alcohol/water solution, formaldehyde was added, and the solution was stirred. Ammonia was then added, and the solution was left for 2 days at room temperature under a static condition. In all runs, the volume of alcohol/water solvent and resorcinol and formaldehyde concentrations were held constant of 50 mL and 0.1 and 0.2 mol/L, respectively. Thus, the alcohol and ammonia concentrations were adjusted from 0 to 98 vol % and from 0.05 to 0.6 mol/L, respectively. Polycondensation reaction occurred, and a suspension of resorcinol resin particles was obtained. The suspension was centrifuged at 3000 rpm for 30 min. The resultant sample was not washed during separation from the mixture. The sample was then dried at 85 °C followed by heat treatment under nitrogen atmosphere at 100–800 °C for 1 h.

2.3. Characterization. Scanning electron microscopy (SEM) images were recorded on a VE-8800 Keyence microscope at an acceleration voltage of 5 kV. Field emission scanning electron microscopy (FESEM) images were recorded on a JEOL JSM-6700 microscope at an acceleration voltage of 5 kV. The diameters of more than 200 particles in the SEM or FESEM images were measured to determine average particle size, d_n, and coefficient of variation, C_v, defined by the following equations:

$$d_n = \sum n_i d_i / \sum n_i \quad (1)$$

$$C_v = 100\sqrt{\sum (d_i - d_n)^2 / \sum n_i}\,/d_n \quad (2)$$

Average particle size was also determined using a ELS-8000 (Otsuka Electronics) dynamic light scanning (DLS) system. Powder X-ray diffraction (PXRD) patterns were recorded on a RINT-TTR III Rigaku diffractometer using Cu Kα radiation with λ = 1.5418 Å. The copper anode was operated at 40 kV and 20 mA. Carbonization was performed by thermogravimetric analysis (TGA) using a DTG-50 (Shimadzu Co.). Samples were heated to 800 °C at a heating rate of 5 °C/min under a nitrogen flow (100 mL/min) or in air. The nitrogen adsorption/desorption isotherms were measured at 77 K using a BELSORP-max instrument (Bel Japan), and the surface area found using the Brunauer–Emmett–Teller (BET) method. The linear region of the *t*-plot method was used to determine the specific external surface area and the specific micropore volume.

Electrochemical measurements consisted of cyclic voltammetry (CV) experiments using a charge–discharge apparatus (HX5000, Hokuto Denko). The electrodes were prepared by mixing resultant carbon spheres with 10 wt % of polytetra-

dx.doi.org/10.1021/jp308415s | J. Phys. Chem. C 2012, 116, 26791–26799

fluoroethylene as binder and 10 wt % of carbon black. The electrode mass was pressed into 10−20 mg pellets. The electrochemical behavior of the carbon electrode was analyzed with a three-electrode configuration in aqueous 1 M H_2SO_4 electrolyte solutions. A Pt wire and Ag/AgCl were used as the counter and reference electrodes, respectively.

3. RESULTS AND DISCUSSION

Figures 1A−F show the photographs of the solutions with time after the addition of ammonia. The solutions were left for 2 min at room temperature, during which they became clouded. Figures 1a−f show the FESEM images of the products prepared by drying of a drop of the mixtures on the silicon substrate. By drying of a drop of the mixtures left for 2 min on the silicon substrate, the amorphous solids were obtained. After 5 min, white mixtures were obtained. When dried, the aggregate composed of approximately spherical particles were obtained. These results suggest that unreacted monomer or oligomers exists in the solution and are deposited during drying process. Thus, the amorphous or aggregated solids were obtained. On the other hand, the isolated spherical particles were obtained from the dried drop of mixtures left for 24 h. Figure SI1 shows the time course of particle size of the resorcinol/formaldehyde resin spheres. The change in average particle size was determined using DLS. The particle size stopped increasing after 20 h.

Figures 2a−g show FESEM images of resorcinol/formaldehyde resin particles prepared at different ethanol concentrations. With ethanol the only solvent in the reaction mixture, coagulation of particles occurred and polydisperse particles were obtained. Higher monodispersity was achieved by combining ethanol and water. The adhesion of resorcinol/formaldehyde resin to the reactor wall was scarcely observed. For ethanol concentrations ranging from 0 to 80 vol %, the particles were isolated and of uniform size. Figure 2h shows the variation in the d_n and C_v as a function of ethanol concentration. The d_n and C_v values varied from 420 to 1090 nm and from 4.8 to 10.3%, respectively. At an ethanol concentration of 60 vol %, the particles were isolated and of more uniform size, with d_n of 670 nm and C_v of 4.8%. The d_n was found to increase with increasing ethanol concentration. In preparation of silica spheres, nucleation and growth of particles have been modeled by a controlled aggregation mechanism of subparticles, a few nanometers in size.[39,40] Colloidal stability, nuclei size, number concentration of nuclei, surface charge, diffusion, and aggregation characteristics are the important parameters. The polymerization mechanism, structure, and properties of the resorcinol/formaldehyde resins are similar to the sol−gel processing of silica.[12] The major reactions between resorcinol and formaldehyde include an addition reaction to form hydroxymethyl derivatives ($-CH_2OH$) and then a condensation reaction of the hydroxymethyl derivatives to form methylene ($-CH_2-$) and methylene ether ($-CH_2OCH_2-$)-bridged compound. Then, small phenolic resin nuclei form continuously during the addition and condensation reaction. At high water concentrations, the number of nuclei generated by the addition and condensation reaction seems to be large, which consequently led to a decrease in the d_n. The nuclei are colloidally unstable, and they will coagulate and form larger units. The aggregated nuclei are stable above a critical size, and their further growth is accomplished by addition of subsequent primary nuclei to the existing "particle" surface of the agglomerates. With ethanol the only solvent, the particle shape tends to deteriorate from that of a perfect sphere due to agglomeration processes not during the early growth period of the nuclei but during the subsequent growth period of the particles.

Figure 3 shows d_n of resorcinol/formaldehyde resin particles prepared using methanol, ethanol, or isopropanol as a function of alcohol concentration. An increase in alcohol concentration led to an increase in the d_n. In these samples the resorcinol/formaldehyde resin particles were isolated. Compared to the particles prepared using methanol or ethanol, a larger d_n was achieved using isopropanol. We speculate that the formation of large particles is due to the swelling of resin particles caused by alcohol that is solubility effect. In addition, the increase in alcohol concentration can be expected to bring about a decrease in electrostatic potential of the particle surface, resulting in the promotion of particle coagulation. The particle sizes of the resorcinol/formaldehyde resin particles were in the order isopropanol > ethanol > methanol. On the other hand, the dielectric constant for alcohols has the order isopropanol (20) < ethanol (25) < methanol (33). This order corresponds to the reverse order of the particle sizes. The number, size, and shape of the units seem to be determined not only by the reaction kinetics but also by different parameters effecting the dispersion stability such as the solvent dielectric constant, pH, ionic strength of the solution, temperature, charges on the particle surface, and so on.

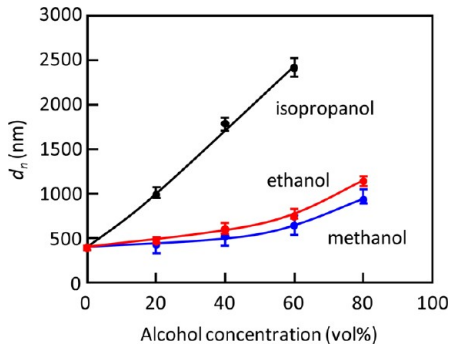

Figure 3. The d_n of resorcinol/formaldehyde resin particles prepared using methanol, ethanol, or isopropanol as a function of alcohol concentration. The products were prepared at ammonia concentration of 0.15 M.

Figures 4a−e show FESEM images of resorcinol/formaldehyde resin particles prepared at different ammonia concentrations. The resorcinol/formaldehyde resin particles prepared at ammonia concentration of 0.07 M were highly dispersed in size and aggregated. On the other hand, the particles prepared at an ammonia concentration more than 0.11 M were highly monodispersed in size and isolated. Figure 4f shows d_n of resorcinol/formaldehyde resin particles as a function of ammonia concentration. The d_n was observed to decrease with increasing ammonia concentration. Polycondensation rate of resorcinol with formaldehyde was increased with ammonia concentration. At high ammonia concentrations, the number of nuclei generated by the polycondensation reaction seems to be large, which consequently led to a decrease in the d_n. In addition, the decrease in d_n is attributed to an increase in the electrostatic surface potential of the resin particles due to an increase in ammonia concentration. The products prepared at ethanol concentration of 40 vol % and ammonia concentration of 0.15 M exhibit ordered close-packed arrangement of

dx.doi.org/10.1021/jp308415s | J. Phys. Chem. C 2012, 116, 26791−26799

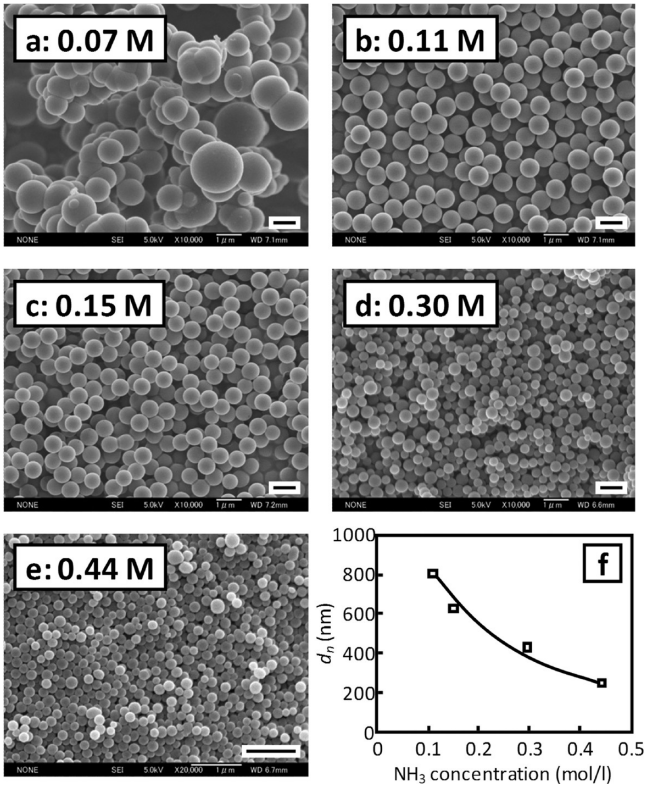

Figure 4. FESEM images of resorcinol/formaldehyde resin particles prepared at different ammonia concentrations (a–e: scale bar; 1 μm). Effect of ammonia concentration on the d_n of spherical particles (f). The products were prepared at ethanol concentration of 40 vol %.

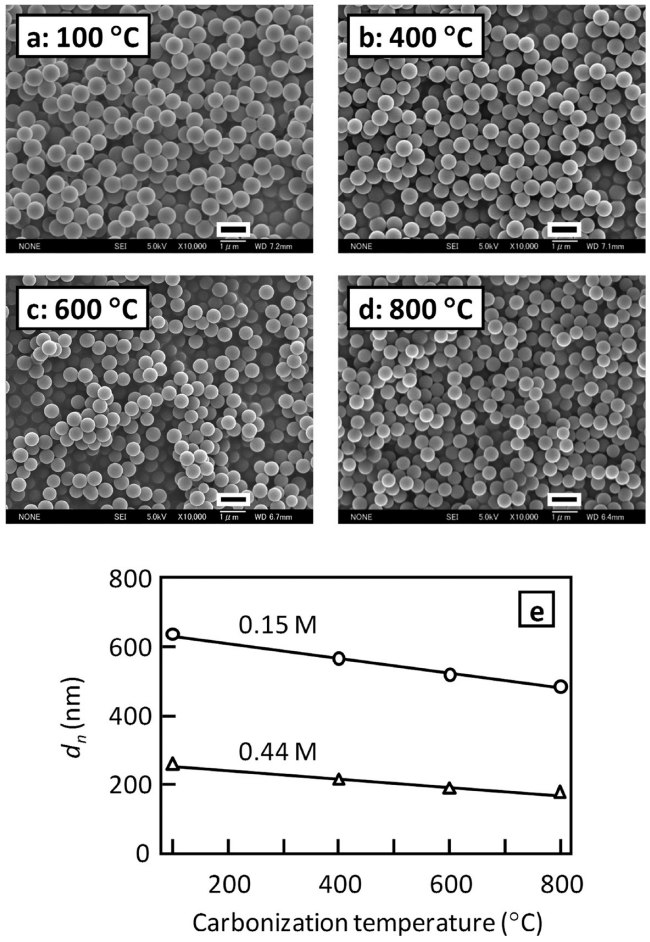

Figure 5. FESEM images of particles carbonized at different temperatures (a–d). The products were prepared at ethanol concentration of 40 vol % and ammonia concentration of 0.15 M. Effect of carbonization temperature on the d_n of spherical particles prepared at ammonia concentration of 0.15 and 0.44 M (e).

resorcinol/formaldehyde resin and carbon colloids over a sample area of about several micrometers (Figure SI2). When the resorcinol/formaldehyde resin spherical particles with C_v of less than 10% were obtained, the colloidal crystallization easily occurred simply by solvent evaporation. Of particular interest is that the ammonia concentration dependence on d_n was completely opposite to that of the well-known Stöber method[28−30] and related method[35] for silica and resorcinol/formaldehyde sphere preparation, respectively. Liu et al. have reported that the diameter of resorcinol/formaldehyde spheres increased from 520 to740 nm with increasing the ammonia concentration from 0.0529 to 0.1587 M. Unfortunately, the direct comparison with Liu's data is difficult because our synthesis does not require the hydrothermal procedure and is performed at up to 4 times higher ammonia concentration. The relationship between d_n and catalyst concentration which observed for the formation of small particles in resorcinol/formaldehyde solutions behaves analogously to the fundamental basis valid in the regime of monolithic gel formation rather than the behavior of Stöber method. In general, the primary particles of resorcinol/formaldehyde aerogels are getting smaller with the synthesis parameters approaching the gelation limit.[34] Increasing the catalyst concentration leads to formation of smaller primary particles and lower reactant mass content is necessary to disperse the particles in isolation. Further work will be undertaken to understand the opposite ammonia dependence on d_n observed for silica and resorcinol/formaldehyde sphere preparation.

The effect of calcination temperature on the particle shape and size is shown in Figure 5. Figure 6 shows the size distributions of final particles carbonized at 800 °C. The particle size did decrease and shrinkage percentage of the particles carbonized at 800 °C was calculated to be 25%. The TGA trace exhibited a weight loss of 55% (Figure SI3). However, the shape and C_v of the particles were maintained after carbonization even at 800 °C. Figure SI4 shows wide-angle PXRD patterns and Raman spectra of the particles carbonized at 400, 600, and 800 °C. These results indicate that the particles carbonized even at 800 °C consist of imperfect graphenes of a very small size. A micropore is the space between the nanographenes. There is no large difference in wide-angle PXRD patterns between the carbonized particles with different d_n (Figure SI5). Nitrogen adsorption/desorption measurements were performed to investigate the pore structure of the carbon spherical particles. Adsorption/desorption isotherms behavior of the carbon spheres shown in Figure 7 yield typical type I curves which reveals their microporous nature. No large difference in isotherm type was observed between the carbon spheres with different d_n. On the other hand, with a decreasing d_n, the capillary condensation steps at P/P_0 around 0.9 increase, which may be result of the interparticle porosity among the reduced-size particles. Table 1 summarizes the results of the structure analysis. The specific surface area, pore volume, average particle size, and coefficient of variation. There is no large difference in the BET surface areas and micropore volumes among the different-sized carbon

dx.doi.org/10.1021/jp308415s | J. Phys. Chem. C 2012, 116, 26791−26799

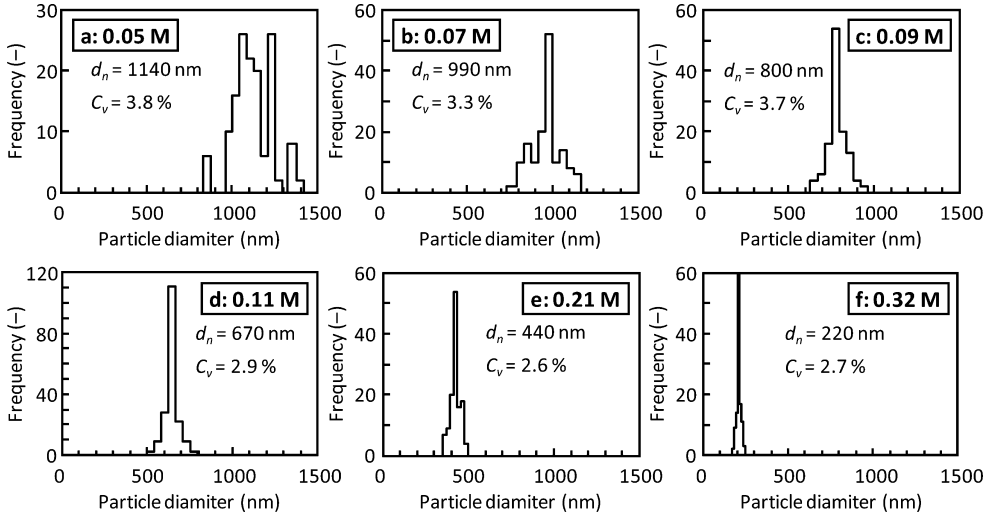

Figure 6. Particle size distributions of final carbon spheres prepared at different ammonia concentrations. The products were prepared at ethanol concentration of 60 vol % and carbonized at 800 °C.

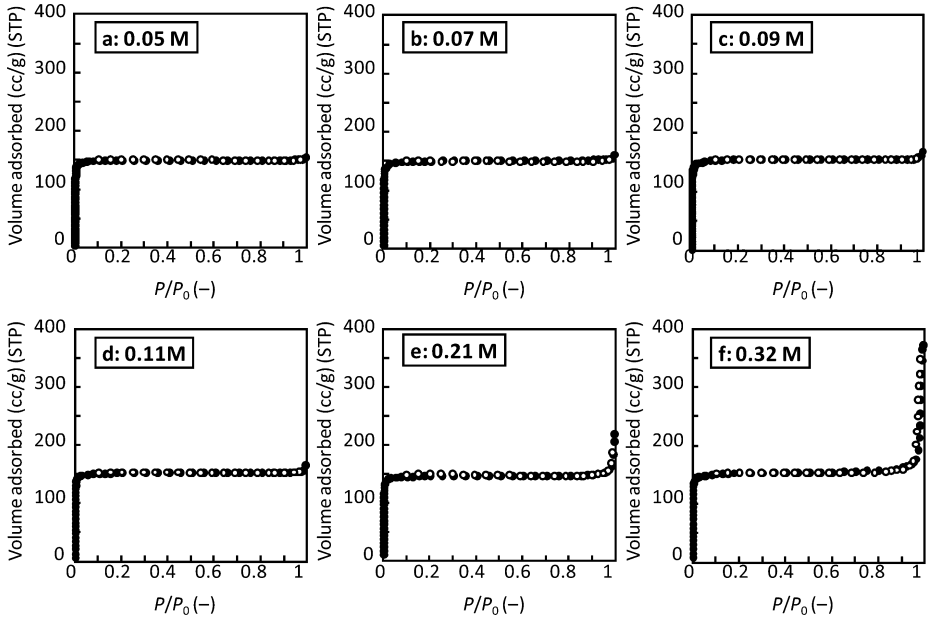

Figure 7. Nitrogen adsorption/desorption isotherms of final carbon spheres prepared at different ammonia concentrations. The products were prepared at ethanol concentration of 60 vol % and carbonized at 800 °C.

Table 1. Structure Characteristics and Capacitance of Carbon Spheres Prepared at Different Ammonia Concentrations[a]

concn of ammonia (M)	d_n[b] (nm)	V_t[c] (cm^3/g)	V_{micro}[d] (cm^3/g)	S_t[e] (m^2/g)	S_{ext}[f] (m^2/g)	C[g] (F/g)	C_s[h] ($\mu F/cm^2$)
0.05	1140	0.23	0.23	800	3.3	36	4.5
0.07	990	0.23	0.23	800	4.4	40	5.0
0.09	800	0.25	0.23	820	5.6	105	12.8
0.11	670	0.25	0.23	820	11.2	128	15.6
0.21	440	0.34	0.23	780	13.4	148	19.0
0.32	220	0.58	0.23	800	19.9	196	24.5
0.42	(280)	0.48	0.23	830	14.7	126	15.2
0.53	(260)	0.49	0.23	820	14.2	115	14.0
0.64	(260)	0.48	0.23	840	14.7	122	14.5

[a]The carbonization temperature was 800 °C. [b]Primary particle size of agglomerated particles is enclosed in parentheses. [c]Total pore volume calculated as the amount of nitrogen adsorbed at a relative pressure of 0.99. [d]Micropore volume calculated from the $V-t$ plot method using the de Boer equation, $t/Å = \sqrt{[13.99/(\log(P_0/P) + 0.0340)]}$; $V_{micro} = 0.001547I$, where I represents the Y-intercept in the $V-t$ plot. [e]Total surface area calculated using the BET method. [f]External surface area calculated from the $V-t$ plot method. [g]Specific capacitance at potential scan rate of 1 mV/s calculated using the CV method. [h]Capacitance per surface area.

dx.doi.org/10.1021/jp308415s | J. Phys. Chem. C 2012, 116, 26791−26799

spheres. On the other hand, the specific external surface area increases with decreasing the d_n. The external surface areas of aggregated spheres are smaller than that of isolated spheres. These results indicate that the monodisperse carbon spheres with only difference in d_n could be obtained. Figure 8 shows the

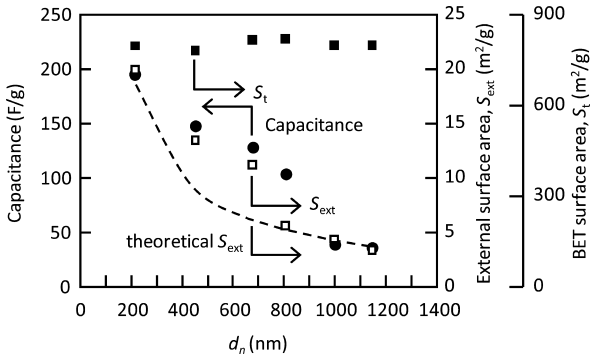

Figure 8. Effect of the particle size on specific surface area, external surface area, and capacitance. Dashed line is the theoretical external surface area calculated using d_n and $\rho_{particle}$ assuming a perfect spherical particle. The capacitance was calculated from CV curve at potential scan rate of 1 mV/s.

variations of the external surface area of the carbon spheres as a function of d_n. Assuming spherical particles external surface area is reciprocal to the d_n; this quantity can be calculated from the particle density $\rho_{particle}$ and the density of nonporous carbon ρ_{carbon} = 2.2 g/cm^3 as follows:

$$d_n = \frac{6}{S_{ext}\rho_{particle}} \quad (3)$$

$$\rho_{particle} = \frac{1}{V_{micro} + 1/\rho_{carbon}} \quad (4)$$

The measured external surface areas of monodisperse carbon spheres were higher than that of calculated from the above equations, indicating that the carbon spheres were fully isolated and have somewhat rough surface.

The electrochemical performance for the microporous carbon spheres was evaluated with a three-electrode cell in an aqueous electrolyte (1 M H_2SO_4) at 25 °C. Electrode sheets for the working electrodes were prepared by mixing the microporous carbon spheres with carbon black and polytetrafluoroethylene. In addition, the electrodes were prepared by pressing procedure to neglect the collector/electrode contact resistance. Figure SI6 shows the cyclic voltammograms of the microporous carbon spheres scanned at varying rates. The voltammograms of smaller carbon spheres were nearly rectangular, which is characteristic of an ideal capacitor. However, the voltammograms of larger carbon spheres were distorted rectangular shape. With an increase in the potential scan rate, the charge transportation resistance became a dominant force in distorting the rectangular shape of the voltammograms. Figure 8 shows the variations of the capacitances of the carbon spheres as a function of d_n. Of particular interest is that the capacitance increased with decreasing d_n although there is no large difference in microporous structure. In addition, the monodisperse carbon spheres with 220 nm in diameter exhibited high specific capacitance 196 F/g and interfacial capacitance 24.5 μF/cm^2. The capacitance values reported in this study correspond to a single electrode. On the other hand, the agglomerated carbon spheres with primary particle size of 260–280 nm exhibited low specific and interfacial capacitances (Table 1). In addition, the capacitive properties of the agglomerated carbon spheres were reproduced within ±18% for different samples while the reproducibility was ±7% for the use of monodisperse carbon spheres. The low reproducibility may be attributed to unstable in mixing characteristic of agglomerated spheres with binder and carbon black in the electrode preparation.

The capacitance variation with the potential scan rate is an important issue in high-rate capacitors. Figure 9 shows the scan

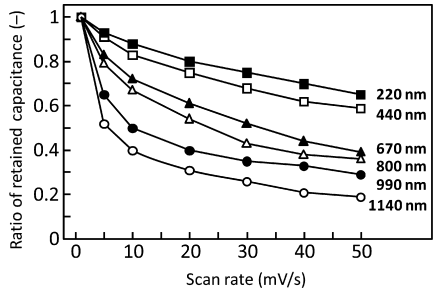

Figure 9. Capacitance at different potential scan rates for different-sized carbon spheres.

rate dependence of the relative capacitance. The capacitance decreased with increasing the scan rate. However, the capacitance decrease was less sensitive for smaller carbon spheres. It is still unclear at this stage which factor, electronic or ionic conductivity or both, enhanced the capacitance and high-rate performance.

The electrochemical impedance technique, which distinguishes the resistance and capacitance of devices, revealed the resistance of the capacitor cells in the double layer formation on the carbon electrodes.[41,42] Figure 10 shows Nyquist plots of the electrochemical impedance spectra of the different-sized carbon spheres. At the high–medium frequency region, all carbon spheres exhibit a depressed semicircle, then straight lines nearly vertical to the realistic impedance axis when frequency is lower than the knee frequency. An electrode/electrolyte interface can be presented by equivalent circuit involving some electronic elements when it is analyzed by electrochemical impedance spectroscopy. Typical equivalent circuit for EDLCs is shown in Figure 10. When the charge transfer resistance R_{ct} and mass transport impedance Z_{mt} are assumed for the electrode, the equivalent circuit involves the series of R_{ct} and Z_{mt}, and the series element is connected in parallel with the electric double layer capacitance C_{dl}. In addition, they are connected in series with the solution resistance R_{sol}. At high frequency, the impedance can be simplified as follows:[42]

$$(\mathrm{Re}(Z) - R_{sol} - R_{ct}/2)^2 + \mathrm{Im}(Z)^2 = (R_{ct}/2)^2 \quad (5)$$

The intercept of the curve with the real axis gives an estimation of R_{sol}. In addition, this means that the semicircle diameter is R_{ct}. The semicircle does not depend on C_{dl}. In this case, we used R_{sol} to represent the migration of electrolyte ions in the bulk solution. Thus, it is nearly constant with the same electrolyte condition. Z_{mt} is used to represent the ion diffusion within the micropores. R_{ct} includes the bulk carbon, grain boundary, and interface resistances. The interfaces are at the electrode/collector and at the electrolyte/external surface of carbon spheres. There is no large difference in the bulk carbon

dx.doi.org/10.1021/jp308415s | J. Phys. Chem. C 2012, 116, 26791–26799

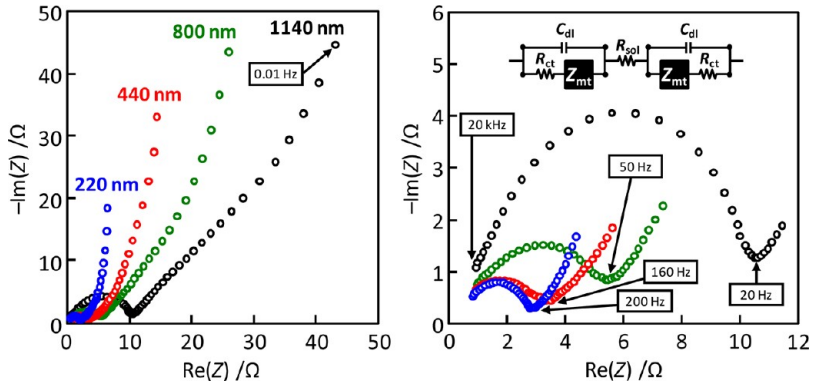

Figure 10. Complex-plane Nyquist plots in the frequency ranging from 10 mHz to 20 kHz for different-sized carbon spheres in H_2SO_4 electrolyte.

and electrode/collector interface resistances. Then, R_{ct} depends on the interface resistance at the electrolyte/external surface of carbon spheres. The semicircle diameter reflects R_{ct} which is strongly dependent on the area of contact between the external surface of carbon spheres and electrolyte solution, and electron conduction abilities can be used to estimate the formation rate of the double layer. As revealed by the semicircle, R_{ct} decreased with decreasing d_n, in good agreement with CV results. At lower frequency, all carbon spheres exhibit the straight line which is the capacitive behavior. The deviation from the vertical line is attributable to inner-micropore diffusion resistance Z_{mt} for electrolyte ions. The advantage of using impedance is that it can separate these elementary steps. The electrochemical impedance spectra demonstrated that the larger carbon spheres have inferior mass transport ability because of the long diffusion length. The wettability with electrolyte and mass transport ability decreased with decreasing external surface area and longer diffusion length of carbon spheres. Then, the capacitance and high-rate performance could be improved by reducing d_n.

4. CONCLUSIONS

We have presented a simple and straightforward method for the preparation of monodisperse carbon spheres by the fabrication and subsequent carbonization of spherical resorcinol/formaldehyde resin particles. The carbon spheres are highly monodisperse and possess homogeneous micropore structure. In addition, the diameters of the carbon spheres can be tuned in the range 220−1140 nm by adjusting the ammonia concentration. Thus, the carbon spheres are meeting the high quality standards of commonly used polymer and silica particles and can be applied for a wide range of applications under severe conditions in which the polymer and silica are chemically damaged. The monodisperse carbon spheres were used as model materials to investigate the relationship between the particle size and the electrochemical capacitance in an aqueous electrolyte solution. The wettability of the electrolyte solution to the carbon spheres and mass transport ability within the micropores were measured by an electrochemical impedance method. The smaller carbon spheres showed the higher capacitance and superior high-rate performance although there is no large difference in the internal pore structure such as surface area and micropore volume. The electrochemical impedance spectroscopy demonstrated that the reducing the particle size and highly monodispersity in both size and shape were effective at reducing mass transport and charge transfer resistances and improving EDLC performance reliability.

■ ASSOCIATED CONTENT

Supporting Information

Change in d_n measured using DLS (Figure SI1), FESEM images (Figure SI2), TGA curves (Figure SI3), PXRD patterns and Raman spectra (Figure SI4), PXRD patterns (Figure SI5), and CV profiles (Figure SI6). This material is available free of charge via the Internet at http://pubs.acs.org.

■ AUTHOR INFORMATION

Corresponding Author

*E-mail shun_tnk@kansai-u.ac.jp; tel +81 (0)6 6368 0851; fax +81 (0)6 6388 8869.

Notes

The authors declare no competing financial interest.

■ ACKNOWLEDGMENTS

We are grateful for financial support from the Murata Science Foundation and the A-STEP FS Stage of the Japan Science and Technology Agency (JST).

■ REFERENCES

(1) Kroto, H. W.; Heath, J. R.; O'Brien, S. C.; Curl, R. F.; Smalley, R. E. *Nature* **1985**, *318*, 162−163.
(2) Iijima, S. *Nature* **1991**, *354*, 56−58.
(3) Kyotani, T.; Tsai, L.; Tomita, A. *Chem. Mater.* **1995**, *7*, 1427−1428.
(4) Kyotani, T.; Nagai, T.; Inoue, S.; Tomita, A. *Chem. Mater.* **1997**, *9*, 609−615.
(5) van Blaaderen, A. *Science* **1998**, *282*, 887−888.
(6) Zakhidov, A. A.; Baughman, R. H.; Iqbal, Z.; Cui, C.; Khayrullin, I.; Dantas, S. O.; Marti, J.; Ralchenko, V. G. *Science* **1998**, *282*, 897−901.
(7) Kocirik, M.; Brych, J.; Hradil, J. *Carbon* **2001**, *39*, 1919−1928.
(8) Perpall, M. W.; Prasanna, K.; Perera, U.; DiMaio, J.; Ballato, J.; Foulger, S. H.; Smith, D. W., Jr. *Langmuir* **2003**, *19*, 7153−7156.
(9) Xia, Y.; Mokaya, R. *Adv. Mater.* **2004**, *16*, 886−891.
(10) Tosheva, L.; Parmentier, J.; Valtchev, V.; Vix-Guterl, C.; Patarin, J. *Carbon* **2005**, *43*, 2474−2480.
(11) Lee, K. T.; Lytle, J. C.; Ergang, N. S.; Oh, S. M.; Stein, A. *Adv. Funct. Mater.* **2005**, *15*, 547−556.
(12) Pekala, R. W. *J. Mater. Sci.* **1989**, *24*, 3221−3227.
(13) Pekala, R. W.; Alviso, C. T.; Kong, F. M.; Hulsey, S. S. *J. Non-Cryst. Solids* **1992**, *145*, 90−98.
(14) Ryoo, R.; Joo, S. H.; Jun, S. *J. Phys. Chem. B* **1999**, *103*, 7743−7746.
(15) Lee, J.; Yoon, S.; Hyeon, T.; Oh, S. M.; Kim, K. B. *Chem. Commun.* **1999**, 2177−2178.
(16) Tanaka, S.; Nishiyama, N.; Egashira, Y.; Ueyama, K. *Chem. Commun.* **2005**, 2125−2127.

(17) Tanaka, S.; Katayama, Y.; Tate, M. P.; Hillhouse, H. W.; Miyake, Y. *J. Mater. Chem.* **2007**, *17*, 3639−3645.
(18) Tanaka, S.; Doi, A.; Nakatani, N.; Katayama, Y.; Miyake, Y. *Carbon* **2009**, *47*, 2688−2698.
(19) Tanaka, S.; Nakatani, N.; Doi, A.; Miyake, Y. *Carbon* **2011**, *49*, 3184−3189.
(20) De Heer, W. A.; Ugarte, D. *Chem. Phys. Lett.* **1993**, *207*, 480−486.
(21) Wang, Z. L.; Kang, Z. C. *J. Phys. Chem. B* **1996**, *100*, 17725−17731.
(22) Wang, Z. L.; Kang, Z. C. *Carbon* **1997**, *35*, 419−426.
(23) Zhong, Z. Y.; Chen, H. Y.; Tang, S. B.; Ding, J.; Lin, J. Y.; Tan, K. L. *Chem. Phys. Lett.* **2000**, *330*, 41−47.
(24) Miao, J. Y.; Hwang, D. W.; Narasimhulu, K. V.; Lin, P.-I.; Chen, Y.-T.; Lin, S.-H.; Hwang, L.-P. *Carbon* **2004**, *42*, 813−822.
(25) Kawaguchi, H. *Prog. Polym. Sci.* **2000**, *25*, 1171−1210.
(26) Ballauff, M.; Lu, Y. *Polymer* **2007**, *48*, 1815−1823.
(27) Kim, J.-W.; Suh, K.-D. *J. Ind. Eng. Chem.* **2008**, *14*, 1−9.
(28) Stöber, W.; Fink, A.; Bohn, E. *J. Colloid Interface Sci.* **1968**, *26*, 62−69.
(29) Fedeyko, J. M.; Rimer, J. D.; Lobo, R. F.; Vlachos, D. G. J. *J. Phys. Chem. B* **2004**, *108*, 12271−12275.
(30) Budny, A.; Novak, F.; Plumeré, N.; Schetter, B.; Speiser, B.; Straub, D.; Mayer, H. A.; Reginek, M. *Langmuir* **2006**, *22*, 10605−10611.
(31) Yokoi, T.; Sakamoto, Y.; Terasaki, O.; Kubota, Y.; Okubo, T.; Tatsumi, T. *J. Am. Chem. Soc.* **2006**, *128*, 13664−13665.
(32) Friedel, B.; Greulich-Weber, S. *Small* **2006**, *2*, 859−863.
(33) Dong, Y.-R.; Nishiyama, N.; Egashira, Y.; Ueyama, K. *Ind. Eng. Chem. Res.* **2008**, *47*, 4712−4718.
(34) Scherdel, C.; Scherb, T.; Reichenauer, G. *Carbon* **2009**, *47*, 2244−2252.
(35) Liu, J.; Qiao, S. Z.; Liu, H.; Chen, J.; Orpe, A.; Zhao, D. Y.; Lu, G. Q. *Angew. Chem., Int. Ed.* **2011**, *50*, 5947−5951.
(36) Choma, J.; Jamiola, D.; Augustynek, K.; Marszewski, M.; Gao, M.; Jaroniec, M. *J. Mater. Chem.* **2012**, *22*, 12636−12642.
(37) Zuleta, M.; Bursell., M.; Bjornbom, P.; Lundblad, A. *J. Electroanal. Chem.* **2003**, *549*, 101−108.
(38) Zuleta, M.; Bjornbom, P.; Lundblad, A.; Nurk, G.; Kasuk, H.; Lust, E. *J. Electroanal. Chem.* **2006**, *586*, 247−259.
(39) Bogush, G. H.; Zukoski, C. F., IV *J. Colloid Interface Sci.* **1991**, *142*, 1−18.
(40) Bogush, G. H.; Zukoski, C. F., IV *J. Colloid Interface Sci.* **1991**, *142*, 19−34.
(41) Sugimoto, W.; Iwata, H.; Yokoshima, K.; Murakami, Y.; Takasu, Y. *J. Phys. Chem. B* **2005**, *109*, 7330−7338.
(42) Itagaki, M.; Suzuki, S.; Shitanda, I.; Watanabe, K. *Electrochemistry* **2007**, *75*, 649−655.